Microwave Imaging by Mixed-Order Discontinuous Galerkin Contrast Source Inversion

Ian Jeffrey[*1], *Amer Zakaria*[1] *and Joe LoVetri*[1]

[1] Electrical and Computer Engineering, E2-390 EITC, 75A Chancellor's Circle, University of Manitoba, Winnipeg, MB, Canada, R3T 5V6. Ian.Jeffrey@umanitoba.ca, Amer.Zakaria@umanitoba.ca, Joe.LoVetri@umanitoba.ca

Abstract

Recent developments in microwave imaging algorithms have led to contrast source inversion algorithms based on finite-element method forward solvers. The resulting algorithms are flexible in their ability to support a variety of microwave imaging environments, including metallic boundaries of practically arbitrary shape. One limitation of low-order finite-element based imaging algorithms is that, unless an explicit dual mesh scheme is imposed, the discretization of the contrast and contrast sources is implied by the mesh that describes the underlying field discretization. High-order expansions for the fields, contrasts and contrast sources overcoming this deficiency. In this work we present a high-order contrast source inversion method for dielectric targets that supports distinct expansion orders for the fields, contrasts and contrast sources. High-order expansions for the contrasts essentially decouples the image reconstruction from the underlying mesh discretization. The field solver is based on a high-order frequency-domain discontinuous Galerkin formulation of Maxwell's curl equations. Results presented for both numerical and experimentally collected transverse magnetic data-sets illustrate the potential of the proposed method.

1. Introduction

In recent years contrast source inversion (CSI) microwave imaging algorithms based on partial differential equation forward solvers such as the finite-element method (FEM) have gained popularity for solving inverse scattering problems [1], [2], [3]. These methods extend the CSI formulation [4] to be able to accurately model a wide variety of imaging chambers, including those bounded by metallic enclosures. A fully three-dimensional FEM-CSI algorithm is used extensively by the Electromagnetic Imaging Lab (EIL) at the University of Manitoba for a variety of applications including biomedical imaging and grain-storage monitoring [3].

Our experience with FEM-CSI has emphasized one of its fundamental limitations: without introducing an explicit dual grid the image reconstruction voxels are implicitly defined by the mesh used to discretize the electromagnetic fields. One way of overcoming this limitation is to use a high-order forward solver in conjunction with high-order expansions for the contrasts and contrast sources. Using this approach the reconstruction procedure is not limited by contrast reconstructions that are piecewise constant on each voxel. Instead, the high-order nature of the reconstruction algorithm permits variation within each voxel, decoupling the image from a strict dependence on the mesh geometry. While a high-order FEM formulation is possible, we have chosen to adopt the discontinuous Galerkin method [5], formulated for the time-harmonic Maxwell equations [6], as our forward solver. This choice is based on current and future work which aims to simultaneously image both magnetic and dielectric targets with the hopes of exploiting magnetic nano-particles as microwave contrast agents. This work extends our recent efforts in this area where the same high expansion order was used to represent the fields, contrasts and contrast sources [7]. Here, we permit the order used to represent each of the three quantities to be distinct. The remainder of this paper will formulate the inverse problem of interest, describe the required discontinuous Galerkin (DG) operators and outline the DG-CSI algorithm. Numerical and experimental results for transverse magnetic data-sets are used to illustrate the capabilities of the resulting imaging algorithm.

2. Problem Statement and the Discontinuous Galerkin Operators

Our goal is to derive a flexible mixed-order DG-CSI algorithm for solving a general microwave imaging (MWI) problem for dielectric contrast functions $\chi(\vec{x})$ and electric contrast sources $\vec{w}(\vec{x})$. The contrast and contrast source functions are assumed to be non-zero for positions $\vec{x}$ contained within the *imaging domain* D. The contrast and contrast sources are to be reconstructed from limited knowledge of the the scattered field $\vec{E}^{sct}(\vec{x})$ known at the discrete points that make up the *data domain* S which lies outside of D. Herein we assume that the total field $\vec{E}^{tot}(\vec{x})$ is given by $\vec{E}^{tot} = \vec{E}^{sct} + \vec{E}^{inc}$ where $\vec{E}^{inc}$ is a known incident field that propagates through a constant background medium defined by the permeability of free space μ_0 and a background permittivity ϵ_b. By seeking to reconstruct the contrast χ we are asking to reconstruct the permittivity $\epsilon(\vec{x})$ inside the imaging domain as can be seen by the definitions of the contrast sources and contrasts:

$$\vec{w} \triangleq j\omega\epsilon_b\chi(\vec{x})\vec{E}^{tot}(\vec{x}), \qquad \chi(\vec{x}) \triangleq \frac{\epsilon(\vec{x}) - \epsilon_b}{\epsilon_b}, \tag{1}$$

where ω is the radial frequency and j is the imaginary unit.

978-1-4673-5225-3/14/$31.00 ©2014 IEEE

A full description of the time-harmonic nodal DG solver is beyond the scope of this paper but is summarized as follows: a computational domain Ω is chosen to contain the imaging domain D. The data domain may be internal or external to Ω where in the latter case a Huygen's surface is used to convert fields within Ω to field values on S. The computational domain Ω is partitioned into simplexes over each of which the fields and contrast sources are expanded in terms of nodal Lagrange interpolating polynomials [5]. An expansion order of P is assumed and suppressed for the fields, while an expansion order of Q is assumed and suppressed for the contrast sources. The fields anywhere in Ω can be reconstructed from the global coefficient vector $\underline{\boldsymbol{E}}$ used to store the field expansion coefficients for each field component over each element. Similarly, $\underline{\boldsymbol{w}}$ represents the coefficients of the contrast sources. The field values on S are represented by $\boldsymbol{E}_S$ where the absence of an underline reflects the fact that these are not field coefficients but are field values at a set of points. A frequency-domain nodal DG formulation, analogous to the one developed in [6], can be expressed in operator notation as:

$$\underline{\boldsymbol{E}}^{sct} = \boldsymbol{\mathcal{L}}\left[\underline{\boldsymbol{w}}\right], \quad \underline{\boldsymbol{E}}_D^{sct} = \boldsymbol{\mathcal{L}}_D\left[\underline{\boldsymbol{w}}\right], \quad \boldsymbol{E}_S^{sct} = \boldsymbol{\mathcal{L}}_S\left[\underline{\boldsymbol{w}}\right], \tag{2}$$

where the operator $\boldsymbol{\mathcal{L}}_D$ restricts the field coefficients $\underline{\boldsymbol{E}}_D^{sct}$ to elements contained in D while $\boldsymbol{\mathcal{L}}_S$ accounts for converting the global coefficients in Ω to field values on S. Both $\boldsymbol{\mathcal{L}}_S$ and $\boldsymbol{\mathcal{L}}_D$ arise from linear transformations of $\boldsymbol{\mathcal{L}}$. We note that implied in the notation is the fact that the operator $\boldsymbol{\mathcal{L}} = \boldsymbol{\mathcal{L}}^{[PQ]}$ maps Qth order contrast source coefficients to Pth order field coefficients.

3. The DG-CSI Cost Functional

The inverse scattering problem of interest consists of the imaging domain D being interrogated by N_t indepedently operating transmitters, each of which supports an incident field described by the Pth order expansion coefficients $\underline{\boldsymbol{E}}_t^{inc}$ in Ω. On the data surface S we collect measurment data $\boldsymbol{E}_{S,t}^{sct,meas}$ corresponding to transmitter t and aim to determine the coefficients $\underline{\chi}$ representing an Rth order expansion for $\chi(\vec{x})$ in D. The contrast source inversion (CSI) cost functional is constructed as [1, 4]

$$\mathcal{F}[\underline{\boldsymbol{w}}_1, \ldots \underline{\boldsymbol{w}}_{N_t}, \underline{\chi}] = \mathcal{F}_S[\underline{\boldsymbol{w}}_1, \ldots \underline{\boldsymbol{w}}_{N_t}] + \mathcal{F}_D[\underline{\boldsymbol{w}}_1, \ldots \underline{\boldsymbol{w}}_{N_t}, \underline{\chi}]. \tag{3}$$

The data cost functional $\mathcal{F}_S$ accounts for the discrepancy in the field produced by the contrast source estimates and the measured data:

$$\mathcal{F}_S[\underline{\boldsymbol{w}}_1, \ldots \underline{\boldsymbol{w}}_{N_t}] = \eta_S \sum_{t=1}^{N_t} ||\boldsymbol{\rho}_t||_S^2, \quad \boldsymbol{\rho}_t = \boldsymbol{E}_{S,t}^{sct,meas} - \boldsymbol{\mathcal{L}}_S[\underline{\boldsymbol{w}}_t] \tag{4}$$

where η_S is a normalization factor [4]. The simulated fields $\boldsymbol{\mathcal{L}}_S[\underline{\boldsymbol{w}}_t]$ are Pth order estimates arising from Qth order expansions for the contrast sources. The domain cost functional, $\mathcal{F}_D$, is a regularizer that accounts for the dissimilarity between the contrast sources $\boldsymbol{w}_t$ and the product of field-times-contrast:

$$\mathcal{F}_D[\underline{\boldsymbol{w}}_1, \ldots \underline{\boldsymbol{w}}_{N_t}, \underline{\chi}] = \eta_D \sum_{t=1}^{N_t} ||\underline{\boldsymbol{r}}_t||_D^2, \qquad \underline{\boldsymbol{r}}_t = j\omega\epsilon_b \left(\tilde{\boldsymbol{\mathcal{V}}}^{[PR]}\underline{\chi}\right) \odot \left(\underline{\boldsymbol{E}}_{D,t}^{inc} + \boldsymbol{\mathcal{L}}_D[\underline{\boldsymbol{w}}_t]\right) - \boldsymbol{\mathcal{V}}^{[PQ]}\underline{\boldsymbol{w}}_t \tag{5}$$

where η_D is a normalization factor [4]. In our mixed-order formulation the linear change-of-order operator $\tilde{\boldsymbol{\mathcal{V}}}^{[PR]}$ is used to map order R expansion for the scalar function χ into an order P vector expansion of the same length as $\underline{\boldsymbol{E}}_{D,t}^{inc}$, while $\boldsymbol{\mathcal{V}}^{[PQ]}$ maps order Q vector expansions into order P vector expansions. The Hadamard product $\odot$ is a straightforward way to represent the product of the Pth order contrast coefficients $\boldsymbol{\mathcal{V}}^{[PR]}\underline{\chi}$ with the Pth order total-field coefficients $\underline{\boldsymbol{E}}_{D,t}^{inc} + \boldsymbol{\mathcal{L}}_D[\underline{\boldsymbol{w}}_t]$ in D. It can be shown that this results in the Pth order expansion coefficients for the product $\chi(\vec{x})\boldsymbol{E}^{tot}(\vec{x})$. Consequently we have chosen to evaluate the domain cost functional $\mathcal{F}_D$ in the space of Pth order polynomials. Investigating other choices for this evaluation, such as the space of Rth order polynomials used to represent the contrast $\chi(\vec{x})$ will be the focus of future work. The norm is used to indicate the norm of the function represented by the coefficients $\underline{\boldsymbol{r}}_t$ over D, that is $||\underline{\boldsymbol{r}}_t||_D^2 \triangleq ||\boldsymbol{r}(\vec{x})||_D^2$. The latter can be evaluated by simple sparse linear transformations of $\underline{\boldsymbol{r}}_t$ [1].

The CSI algorithm proceeds by iteratively updating the coefficients for the contrast sources using a conjugate gradient method [1, 4]. Once the contrast sources have been updated, the contrast coefficients $\underline{\chi}$ are analytically recovered from the domain cost functional $\mathcal{F}_D$ via minimization with respect to the contrast. It can be shown that this analytic recovery step is unique for recovering the contrast in the space of Pth order coefficients, *i.e.,* $\boldsymbol{\mathcal{V}}^{[PR]}\underline{\chi}$. In order to recover the contrast coefficients in the space of Rth order polynomials we must use a change-of-order operator:

$$\underline{\chi} = \boldsymbol{\mathcal{V}}^{[RP]}\left(\boldsymbol{\mathcal{V}}^{[PR]}\underline{\chi}\right). \tag{6}$$

This operation is meaningful when $R < P$, that is when trying to limit the reconstruction of the contrast to lower orders than those used to represent the fields. In this sense we can view this operation as a kind of projection-based regularization. For cases when $R > P$ this operator will simply represent the Pth order contrast $\boldsymbol{\mathcal{V}}^{[PR]}\underline{\chi}$ in the space of Rth order polynomials providing no additional regularization.

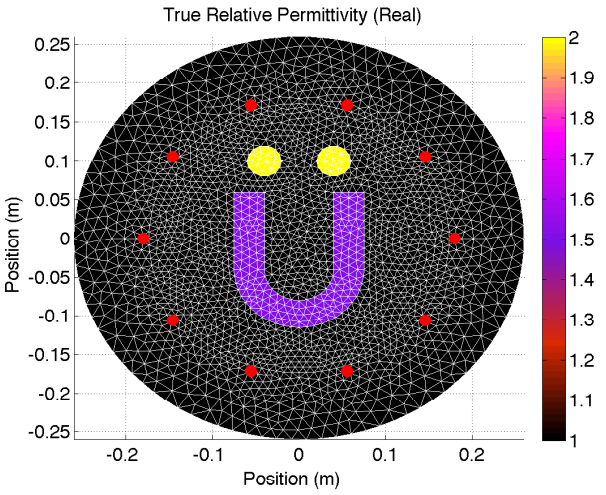

Figure 1: True relative permittivity profile and transmitter/receiver locations (red dots) for the synthetic U-shaped target.

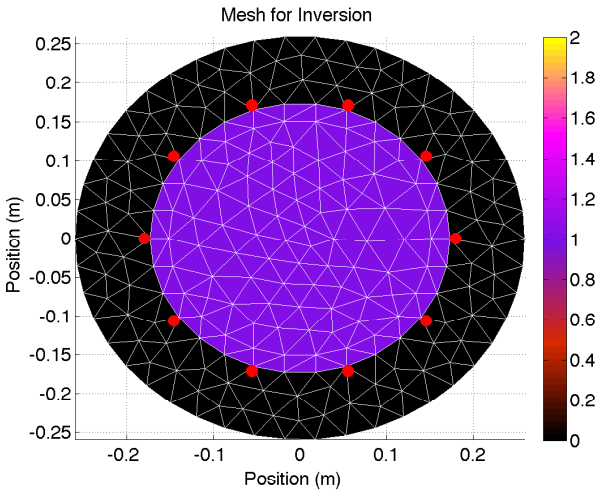

Figure 2: Inversion mesh for the U-shaped target. Imaging domain elements are assigned a value of 1 for identification purposes.

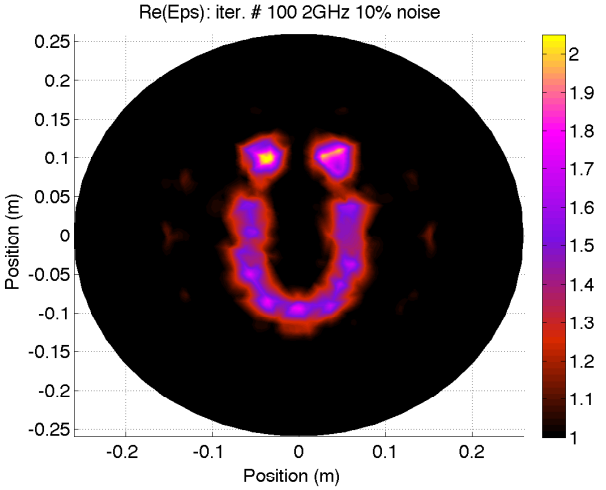

Figure 3: 2nd order reconstruction of the relative permittivity demonstrating mesh dependence due to the coarseness of the inversion mesh.

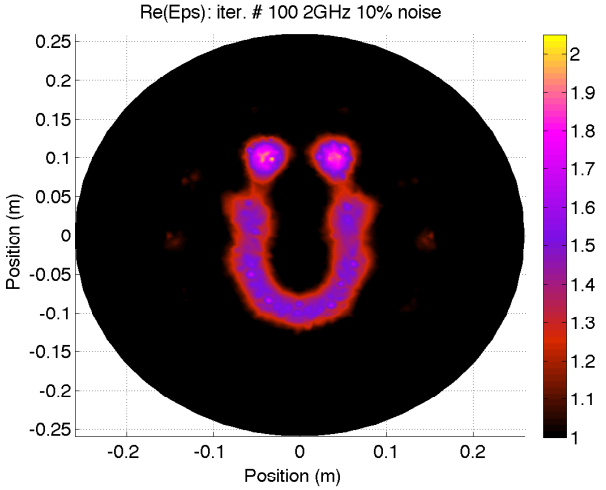

Figure 4: 5th order reconstruction of the relative permittivity shows improved shape capture due to mesh independence.

4. Numerical and Experimental Results

The proposed mixed-order discontinuous Galerkin contrast source inversion algorithm (DG-CSI) will now be illustrated by means of one synthetic and one experimental transverse magnetic imaging problem. We begin with the synthetic example shown in Figure 1, a U-shaped target, having a relative permittivity of 1.5 and accented by an umlaut with a relative permittivity of 2. $N_t = 10$ transmitters were used, equally spaced along a circle of radius 0.18 m shown by the red dots in the figure. Receivers were collocated at the transmitter locations. The DG forward solver was used to generate a 2nd-order accurate field solution on this refined mesh, and the transverse electric field componenet E_z^{sct} was computed at the measurement locations for incident fields radiating at 2 GHz. At this frequency, the diameter of the circle containing the transmitter locations is slightly larger than 2 wavelengths. 10% noise was added to the data. The inversion mesh shown in Figure 2 contains fewer than 10 elements per wavelength and a high-order field solution is adopted. The imaging domain, shown in purple, was selected to be a circle of radius 1.7 m. We selected $P = 5$ as the field order. Image reconstruction after 100 iterations is shown in Figures 3 and 4 for the contrast order $R = 2$ and 5 respectively. In both cases the contrast source order was set to $Q = P$. The 2nd order reconstruction provides a reasonable image but mesh dependence is visible due to the large element sizes and the relatively low reconstruction order. Improved results are obtained for the 5th order reconstruction where the high-order reconstruction compensates for the large elements in the underlying mesh.

The synthetic example chosen is that of two nylon cylinders each having a diameter of 3.81 cm and a length of 44 cm, sufficiently long to assume longitudinal invariance. A dataset at 5 GHz was collected by the Electromagnetic Imaging Lab at the University of Manitoba for a separation distance between the cylinders of 8 mm. Details can be found, for example, in [8]. At 5 GHz the relative permittivity of the cylinders is approximately 3 with a negligible imaginary part. At 5 GHz the

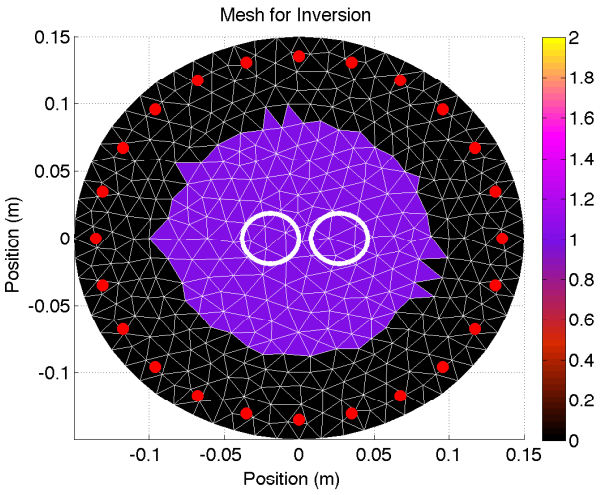

Figure 5: Inversion mesh for the experimental data collected for two nylon cylinders. The cylinder locations are shown by the white circles.

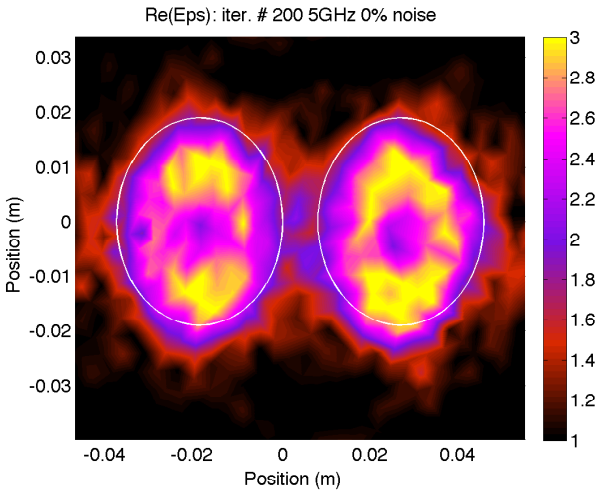

Figure 6: Zoomed view of a 4th order reconstruction of the relative permittivity. Expected locations are shown by circles. Reconstruction is accurate despite the coarse mesh.

computational domain is approximately 5 wavelengths in diameter. The mesh used by the DG-CSI algorithm to invert the data is shown in Figure 5. Reconstruction results for $P = Q = R = 4$ are shown in Figure 6. The location and permttivity of the targets are reconstructed quite well given the coarse nature of the mesh.

5. Conclusions

The proposed mixed-order DG-CSI algorithm supports independent expansion orders for the fields, contrasts and contrast sources and has a demonstrated potential to reduce mesh dependence during the image reconstruction. We are currently working towards extending multiplicative regularization to this high-order formulation in the hopes of improving image reconstruction capabilities. In the future we plan on developing an automated local-order refinement scheme in order to efficiently exploit the high-order capabilities of DG-CSI.

References

[1] A. Zakaria, C. Gilmore and J. LoVetri, "Finite-element contrast source inversion method for microwave imaging," *Inverse Prob.*, vol. 26, no. 11, 2010.

[2] A. Zakaria and J. LoVetri, "Application of multiplicative regularization to the finite-element contrast source inversion method," *IEEE Trans. Antennas Propag.*, vol. 59, no. 9, 2011.

[3] A. Zakaria, I, Jeffrey, and J. LoVetri, "Full-vectorial parallel finite-element contrast source inversion method," *Progress In Electromagnetics Research*, vol. 142, 463-483, 2013.

[4] P. M. van den Berg and R. E. Kleinman, "A contrast source inversion method," *Inverse Prob.*, vol. 13, 1997.

[5] J. S. Hesthaven and T. Warburton, *Nodal Discontinuous Galerkin Methods: Algorithms, Analysis, and Applications*, Springer, 2008.

[6] M. E. Bouajaji, and S. Lanteri, "High order discontinuous Galerkin method for the solution of 2D time-harmonic Maxwell's equations," *Applied Mathematics and Computation*, vol. 219, no. 13, 2013.

[7] I. Jeffrey, A. Zakaria and J. LoVetri, "Discontinuous Galerkin Microwave Imaging," Submitted to *ANTEM 2014 Conference* .

[8] C. Gilmore, P. Mojabi, A. Zakaria, S. Pistorius and J. LoVetri, "On super-resolution with an experimental microwave tomography system." *IEEE Antennas and Wireless Propagation Letters*, vol. 9, pp 393-396, 2010.